Basic parameters of the helium-accreting X-ray bursting neutron star in 4U 1820−30

Valery F. Suleimanov,[1,2,3]⋆ Jari J. E. Kajava,[4,5]⋆ Sergey V. Molkov,[3] Joonas Nättilä,[5,6] Alexander A. Lutovinov,[3] Klaus Werner[1] and Juri Poutanen[5,6]⋆

[1]*Institut für Astronomie und Astrophysik, Kepler Center for Astro and Particle Physics, Universität Tübingen, Sand 1, D-72076 Tübingen, Germany*
[2]*Kazan (Volga region) Federal University, Kremlevskaya street 18, Kazan 420008, Russia*
[3]*Space Research Institute, Russian Academy of Sciences, Profsoyuznaya 84/32, 117997 Moscow, Russia*
[4]*Finnish Centre for Astronomy with ESO (FINCA), University of Turku, Väisäläntie 20, FI-21500 Piikkiö, Finland*
[5]*Tuorla Observatory, Department of Physics and Astronomy, University of Turku, Väisäläntie 20, FI-21500 Piikkiö, Finland*
[6]*Nordita, KTH Royal Institute of Technology and Stockholm University, Roslagstullsbacken 23, SE-10691 Stockholm, Sweden*

ABSTRACT

The ultracompact low-mass X-ray binary 4U 1820−30 situated in the globular cluster NGC 6624 has an orbital period of only ≈11.4 min, which likely implies a white dwarf companion. The observed X-ray bursts demonstrate a photospheric radius expansion phase and therefore are believed to reach the Eddington luminosity, allowing us to estimate the mass and the radius of the neutron star (NS) in this binary. Here, we re-analyse all *Rossi X-ray Timing Explorer* observations of the system and confirm that almost all the bursts took place during the hard persistent state of the system. This allows us to use the recently developed direct cooling tail method to estimate the NS mass and radius. However, because of the very short, about a second, duration of the cooling tail phases that can be described by the theoretical atmosphere models, the obtained constraints on the NS radius are not very strict. Assuming a pure helium NS atmosphere, we found that the NS radius is in the range 10–12 km, if the NS mass is below $1.7\,M_\odot$, and in a wider range of 8–12 km for a higher 1.7–$2.0\,M_\odot$ NS mass. The method also constrains the distance to the system to be 6.5 ± 0.5 kpc, which is consistent with the distance to the cluster. For the solar composition atmosphere, the NS parameters are in strong contradiction with the generally accepted range of possible NS masses and radii.

Key words: stars: neutron – X-rays: bursts – X-rays: individual: 4U 1820−30 – X-rays: stars.

1 INTRODUCTION

Many accreting neutron stars (NSs) in low-mass X-ray binaries (LMXBs) are sources of relatively bright X-ray bursts, extensively investigated by the *Rossi X-ray Timing Explorer (RXTE)* in the past two decades (see, e.g. Galloway et al. 2008). The X-ray bursts are produced by thermonuclear flashes on NS surfaces of the freshly accreted matter from the binary companion (see, e.g. reviews by Lewin, van Paradijs & Taam 1993; Bildsten 1998; Cumming 2004; Strohmayer & Bildsten 2006). The emergent spectra of X-ray bursting NSs are usually well fitted with a blackbody (Galloway et al. 2008) because of the importance of the Compton effect in their atmospheres (London, Howard & Taam 1984; Lapidus, Sunyaev & Titarchuk 1986; London, Taam & Howard 1986; Ebisuzaki 1987; Madej 1991; Pavlov, Shibanov & Zavlin 1991). Some of the power-

ful bursts reach the Eddington luminosity and this fact is very useful for limiting the NSs masses M and radii R (Damen et al. 1990; Lewin et al. 1993; Özel 2006). These bursts demonstrate an appearance of the radius expansion phase (Paczynski & Anderson 1986; Damen et al. 1990; Lewin et al. 1993), and they are called photospheric radius expansion (PRE) bursts.

Masses and radii of NSs comprise important information about the physics of cold superdense matter in their cores (see, e.g. Haensel, Potekhin & Yakovlev 2007; Lattimer & Prakash 2007; Lattimer & Steiner 2014). Properties of such matter are not well understood yet and this issue is known as the problem of the equation of state (EoS). A few years ago, a novel cooling tail method for determination of masses and radii of X-ray bursting NSs was suggested (Suleimanov et al. 2011b). This method is based on the approaches developed before by Ebisuzaki (1987) and van Paradijs et al. (1990), and on modern model atmospheres of X-ray bursting NSs (Suleimanov, Poutanen & Werner 2011a, 2012). It was recently modified to remove some systematic uncertainties present in the original method (Suleimanov et al. 2017). The method assumes

⋆ E-mail: suleimanov@astro.uni-tuebingen.de (VFS); jari.kajava@gmail.com (JJEK); juri.poutanen@utu.fi (JP)

that a burst can be described by a passively cooling uniform NS without any influence of the accreted matter. Such conditions seem to be fulfilled only in PRE bursts taking place during a low/hard persistent state of the host LMXB (Suleimanov et al. 2011b; Kajava et al. 2014; Suleimanov et al. 2016). The method was applied to some X-ray bursts (Suleimanov et al. 2011b; Poutanen et al. 2014; Nättilä et al. 2016). We note, however, that the method can be used for non-PRE bursts during hard persistent state as well (Zamfir, Cumming & Galloway 2012).

The main uncertainty of the method is the chemical composition of the X-ray bursting NS atmosphere. It is mainly determined by the chemical composition of the accreted matter, which is actually unknown, and the results obtained using hydrogen-rich and hydrogen-poor model atmospheres differ significantly (Suleimanov et al. 2011b; Poutanen et al. 2014). There are two reasons for that. First, the model curves w–$w f_c^4$ L/L_{Edd}, which have to be compared with the observed curves K–F_{BB}, depend on the chemical composition. Here, L is the luminosity, L_{Edd} is the Eddington luminosity of the considered NS, K is the normalization factor of a blackbody fitted to the observed spectrum F_E, F_{BB} is the blackbody observed flux and E is the photon energy. The dilution factor w and the colour-correction factor f_c are the parameters of the diluted blackbody spectrum $\mathcal{F}_E \approx w\,\pi B_E(f_c T_{eff})$ fitted to the data. The colour temperature $T_c = f_c\,T_{eff}$ is larger than the effective temperature T_{eff} by the colour-correction factor $f_c > 1$. Secondly, the Eddington luminosity depends on the hydrogen mass fraction X, $L_{Edd} = 4\pi G M c\,(1+z)/0.2(1+X)$, where z is the surface gravitational redshift. As a result, the solution obtained assuming pure helium atmosphere gives twice as large NS radii in comparison with the solution for a pure hydrogen atmosphere.

The photospheric chemical composition of X-ray bursting NSs can be potentially enriched by heavy elements because of thermonuclear burning at the bottom of the accreted envelope (Weinberg, Bildsten & Schatz 2006; in't Zand & Weinberg 2010). To investigate the effect of metal enrichment on the emergent atmosphere spectra, an extensive set of model atmospheres with various heavy element abundances (up to pure iron atmospheres) were recently computed by Nättilä et al. (2015) (see also Rauch, Suleimanov & Werner 2008). The main conclusion of this work is that the colour correction f_c decreased with increasing heavy element abundances at a given relative model luminosity L/L_{Edd}. Importantly, a significant jump in the K–F_{BB} curve has been observed in the X-ray burster HETE J1900.1−2455, which was interpreted as a transition from the metal-enriched photosphere to a photosphere covered by the freshly accreted matter with a solar H/He mix (Kajava et al. 2017). Moreover, an absorption edge was also found in the spectra of HETE J1900.1−2455 at the suggested metal-enriched X-ray burst phase. Unfortunately, relatively little heavy element enhancement (up to ten times solar abundance) cannot be easily detected and it may lead to a large source of systematic uncertainty for NS mass and radius measurements using X-ray bursts. For example, this was the likely reason for the overestimation of the NS radius in 4U 1724−307 by Suleimanov et al. (2011b), when compared with the results obtained later by Nättilä et al. (2016) for a different burst of the same source.

The significant difference between obtained NS radii, when hydrogen-rich and helium-rich model atmospheres are used, offers the possibility to distinguish between NSs accreting matter of corresponding chemical composition. In particular, an acceptable solution for the X-ray bursting NS in 4U 1702−429 was obtained using only a pure helium atmosphere (Nättilä et al. 2016). The orbital period of that system is unknown, and therefore there is

no direct evidence that the system is an ultracompact binary like 4U 1820−30, which is known to have a helium-rich white dwarf companion. However, there is indirect evidence such as a relatively large ratio of the energy release between bursts to the burst fluence ($\alpha \approx 75$), and relatively short burst rise times and flux decay timescales (Galloway et al. 2008). It is very important to apply the direct cooling tail method to the X-ray bursts of 4U 1820−30 to validate the method using a system with a helium-rich companion. This is the main aim of this work.

The ultracompact X-ray binary 4U 1820−30 with an orbital period of 685 s (Stella, Priedhorsky & White 1987) is located in the globular cluster NGC 6624 at a distance of 7.6 ± 0.4 kpc (Heasley et al. 2000; Kuulkers et al. 2003). Most probably, the LMXB 4U 1820−30 is a member of a triple system, as the persistent X-ray flux of the system is modulated with a period of ≈ 171 d (Priedhorsky & Terrell 1984; Chou & Grindlay 2001; Zdziarski, Wen & Gierliński 2007). Thermonuclear X-ray bursts in the system discovered by the *ANS* observatory (Grindlay et al. 1976) occur near the minimum of the persistent X-ray flux (Clark et al. 1977; Chou & Grindlay 2001). It is commonly accepted that the secondary star in the system is a helium white dwarf with a mass of ≈ 0.06–0.07 M$_\odot$ (Rappaport et al. 1987, see, however, Postnov & Shakura 1987; Iben & Tutukov 1991). The hypothesis of an almost pure helium composition of the accreted matter is suggested by a large value of $\alpha \approx 125$–155 obtained by Haberl et al. (1987) using *EXOSAT* observations. A detailed comparison of theoretical predictions derived from thermonuclear flash models with observations was performed by Cumming (2003), who showed that the hydrogen mass fraction in the accreted matter cannot exceed 0.1. One long superburst connected with carbon burning was also detected in the system (Strohmayer & Brown 2002).

Thermonuclear X-ray bursts of 4U 1820−30 were intensively investigated using the *RXTE* observatory (see, e.g. Güver et al. 2010), and the most detailed investigation was made by García, Zhang & Méndez (2013) (see also Kajava et al. 2014). They found 16 short PRE X-ray bursts with a total duration of about 20–30 s and showed that all of them (with one exception) took place in a hard spectral state. Moreover, they demonstrated, that the model curve f_c–L/L_{Edd} computed for pure helium atmospheres describes reasonably well the observed curve $K^{-1/4}$–F_{BB} in the luminosity interval $L/L_{Edd} \sim 0.55$–0.95. Therefore, we can expect that the direct cooling tail method can be used for NS mass and radius determination in this system.

2 ANALYSIS OF THE OBSERVATIONAL DATA

2.1 Persistent emission

We analysed all available *RXTE*/PCA observations of 4U 1820−30 using standard reduction procedures, described in detail in Kajava et al. (2014). There are 16 PCA observations where short PRE X-ray bursts are seen, and they have been studied earlier by García et al. (2013) and Kajava et al. (2014). All observations were divided into 48 s long intervals, making together about 27 000 observing windows. To investigate their spectral properties, the observed energy band was divided into three bands, 3–6 keV, 6–12 keV and 12–25 keV, and the corresponding fluxes F_{3-6}, F_{6-12} and F_{12-25} were estimated using a two-component model described below. Using the soft (SC = F_{3-6}/F_{6-12}) and the hard (HC = F_{12-25}/F_{6-12}) colours, we obtained a colour–colour diagram (Fig. 1), which is similar to those obtained by García et al. (2013) and Kajava et al. (2014). As
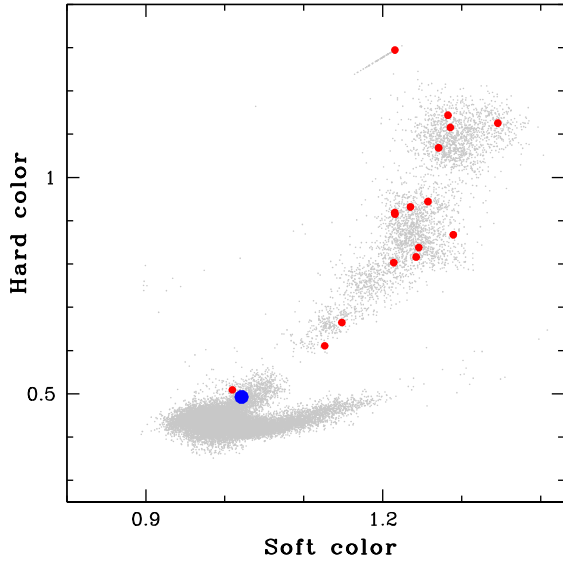
Figure 1. Colour–colour diagram for the persistent spectrum of 4U 1820−30 as observed by *RXTE* in all separate 48-s time windows. The positions of the source before short X-ray bursts are marked by the red dots. The superburst is marked by the large blue circle.
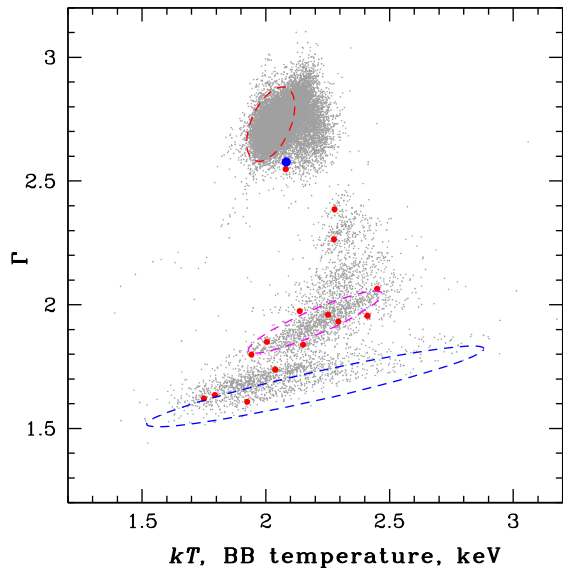

Figure 2. Same as Fig. 1 but for the Γ–kT dependence. The spectra assigned to three different groups are marked by different colour dashed ovals: the top red one represents the soft state, the middle magenta one represents the intermediate state and the bottom blue one represents the hard state.

it was shown in the cited works, the bursts occur predominantly in the hard persistent states (the hard colour is larger than 0.5).

The persistent spectra were analysed using the XSPEC (Arnaud 1996) package and were fitted with a two-component BBODYRAD + POWERLAW model with the main fitting parameters being the blackbody temperature kT and the power-law index Γ. Additionally, the interstellar absorption was accounted for with model WABS with the fixed value of the hydrogen column density of $N_H = 1.6 \times 10^{21}$ cm^{-2} following Costantini et al. (2012). The Γ–kT diagram is shown in Fig. 2. We note that the power-law component dominates in the hard persistent states when the hard colour >0.5 and $\Gamma < 2.5$. The contribution of the blackbody component
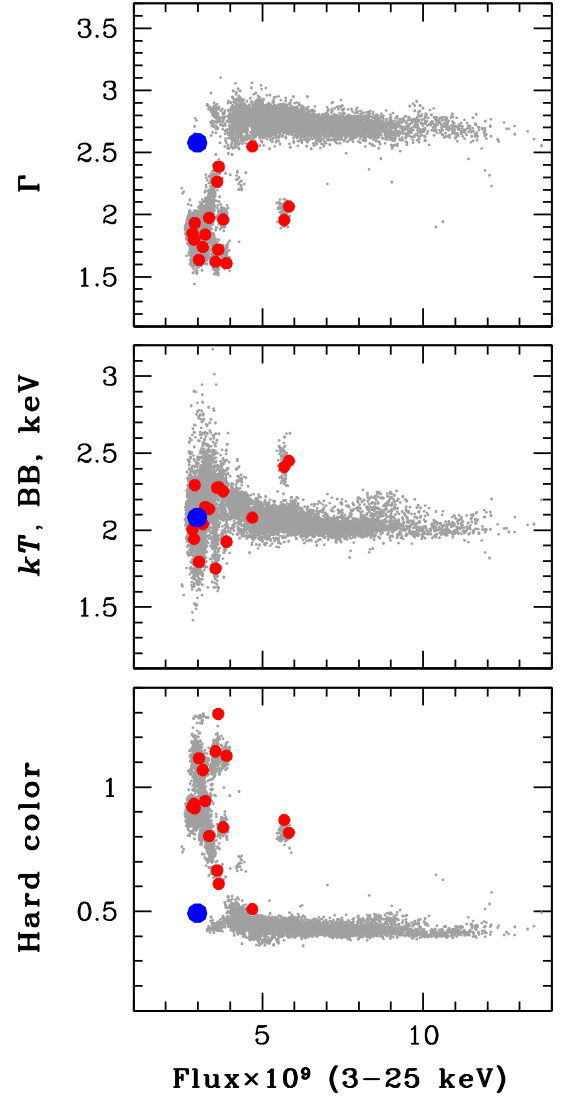

Figure 3. Dependences of Γ, kT and the hard colour on the observed persistent flux (in units of 10^{-9} erg cm^{-2} s^{-1}) in the 3–25 keV band for all 48 s long observing windows of 4U 1820−30. The positions of the source at the time of short X-ray bursts are marked by the red circles.

decreases with a decreasing Γ. As a result, the blackbody temperature becomes very uncertain at low Γ and ranged from 1.5 to 3 keV. On the other hand, the contribution of the power-law component is insignificant in the soft persistent state (the hard colour is less than 0.5) and the spectra are almost blackbodies with temperatures of about 1.9–2.3 keV.

The dependences of three persistent state parameters, kT, Γ and the hard colours on the observed flux in the 3–25 keV band are shown in Fig. 3. This figure confirms a well-known fact that the bursts in 4U 1820−30 take place predominantly at low luminosities in the hard persistent state. However, one *RXTE* observation caught two bursts from the source when it was at a significantly higher luminosity, but still in the hard spectral state. This means that the possibility for the thermonuclear flash depends on the persistent spectral state rather than just on the bolometric luminosity. One possibility is that in the soft state a spreading layer forms in between the NS envelope and the accretion disc, and this layer dissipates a fraction of its rotational energy in the nuclear burning depths (Inogamov & Sunyaev 2010).
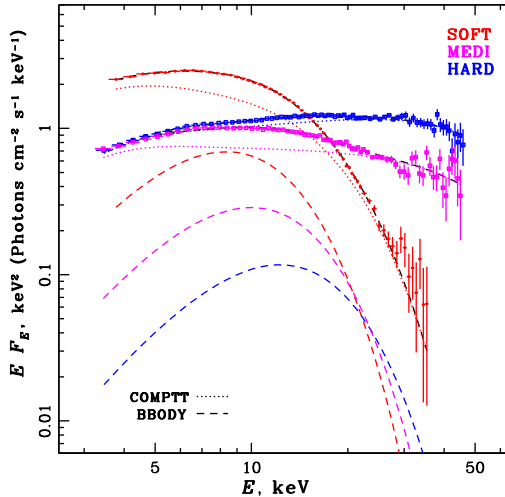
Figure 4. The persistent spectra of the source in three states (soft, intermediate and hard) averaged over some observations within the ovals marked in Fig. 2 together with the best-fitting two-component spectral models.

Table 1. Best-fitting parameters for the averaged spectra of the three persistent spectral states.

Parameter	Soft	Intermediate	Hard
kT	2.20 ± 0.2	2.56 ± 0.15	3.15 ± 0.37
K	8.3 ± 1.2	1.35 ± 0.21	0.24 ± 0.10
kT_0	0.7 ± 0.1	0.76 ± 0.05	0.85 ± 0.02
kT_e	3.6 ± 0.4	12.35 ± 3.1	12.0 ± 1.3
τ_e	4.2 ± 0.9	2.2 ± 0.5	2.77 ± 0.25

Note: kT (keV) and K are the temperature and normalization of the BBODYRAD model. kT_0 is the temperature (keV) of the seed photons, kT_e is the temperature (in keV) of the hot electrons and τ_e is the optical thickness of the electron slab for the COMPTT model. Errors are 1σ.

This extra heat dissipation could lead to steady helium burning and thus cessation of X-ray bursts, as was speculated by in't Zand et al. (2012).

We performed a more detailed study of the persistent spectra. Some of them were summed into three groups shown in the Γ–kT diagram (Fig. 2) by three different colours. They represent the soft, intermediate and hard spectral states. The averaged spectra of these three groups together with the best-fitting models are shown in Fig. 4. The spectra were fitted with the two-component BBODYRAD + COMPTT model and same interstellar absorption as above. The obtained best-fitting parameters are presented in Table 1. We note, however, that this kind of spectral decomposition is ambiguous and the frequency-resolved spectroscopy has to be used to separate reliably different components (see e.g. Gilfanov, Revnivtsev & Molkov 2003; Revnivtsev, Suleimanov & Poutanen 2013).

2.2 Bursts

The light curves of all the short X-ray bursts of 4U 1820−30 are shown in Fig. 5. All the bursts are very short with the bright phase lasting only about 10 s and all of them manifest clear PRE burst features with slightly different PRE phase durations.

The burst spectra were extracted as described in Kajava et al. (2014). The burst light curves (Fig. 5) were divided into about 40 time bins with approximately the same number of photons in each of them. The bin time duration therefore varies from 0.125 s at the brightest phases up to 4 s in the faintest time intervals. The
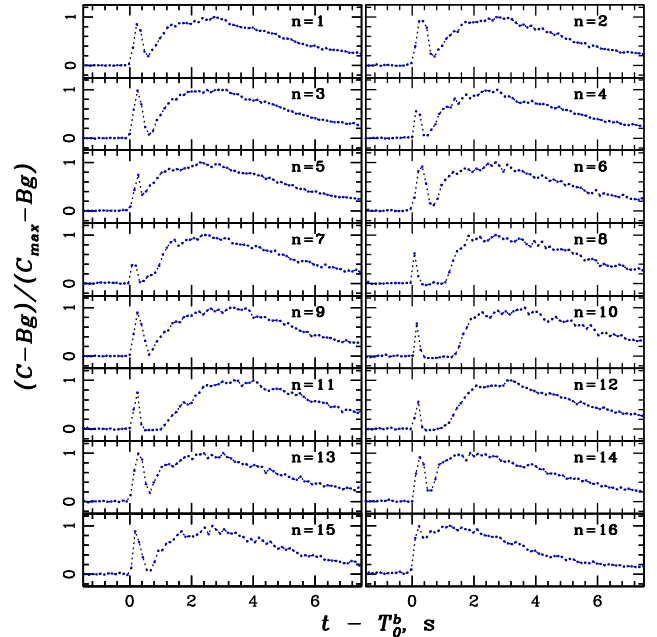

Figure 5. Light curves of the bursts in the energy band 3–25 keV normalized to the maximum with the persistent count rate subtracted as background.

spectrum of each bin was fitted with the BBODYRAD model. The interstellar absorption taken into account with the WABS model at fixed $N_H = 1.6 \times 10^{21}$ cm^{-2}. The burst spectra were also fitted with a slightly higher value of $N_H = 2.5 \times 10^{21}$ cm^{-2} as reported in Güver et al. (2010), but the results have not changed. The same conclusion was reached by García et al. (2013). In addition, in Kajava et al. (2014), we fitted the bursts using N_H as a free parameter, and the results were found to be comparable. Thus, the way in which we model the interstellar absorption does not influence the values of the blackbody model parameters.

What may influence the results is the choice of how we take into account corrections from the persistent spectrum. We used the standard approach, whereby the persistent spectra prior to the bursts were considered as a background and subtracted from the burst spectra. This method ignores the possible changes of the persistent spectra during the bursts (see e.g. Worpel, Galloway & Price 2013, 2015; Ji et al. 2013). We therefore tested the presence of possible persistent spectral variations during the first burst (OBSID: 20075-01-05-00) with the method proposed by Worpel et al. (2013). Here, the persistent emission spectrum is not subtracted as a background, but instead its model spectrum with a free multiplier f_a is added to the burst model spectrum and fitted to the data. In the cooling tail – which we use to constrain the NS parameters – the f_a values were consistent with unity and the improvement to the fit was found to be insignificant. As a consequence, the results did not change from the standard case, and therefore we decided to apply a standard procedure and subtract the persistent spectrum as in Kajava et al. (2014).

An example of such a fit is shown in Fig. 6. The touchdown point, where the blackbody temperature T_{BB} reaches the maximum and the normalization K reaches the minimum, is marked by the left vertical dashed line. The normalization K undergoes clear evolution after the touchdown point. It has a minimum value at the touchdown, then increases up to the maximum value after approximately one second, and then slowly decreases. The maximum value of the normalization approximately corresponds to $kT_{BB} = 2.4$ keV and the blackbody flux $F_{BB} = 0.38 \times 10^{-7}$ erg s^{-1} cm^{-2}. These values
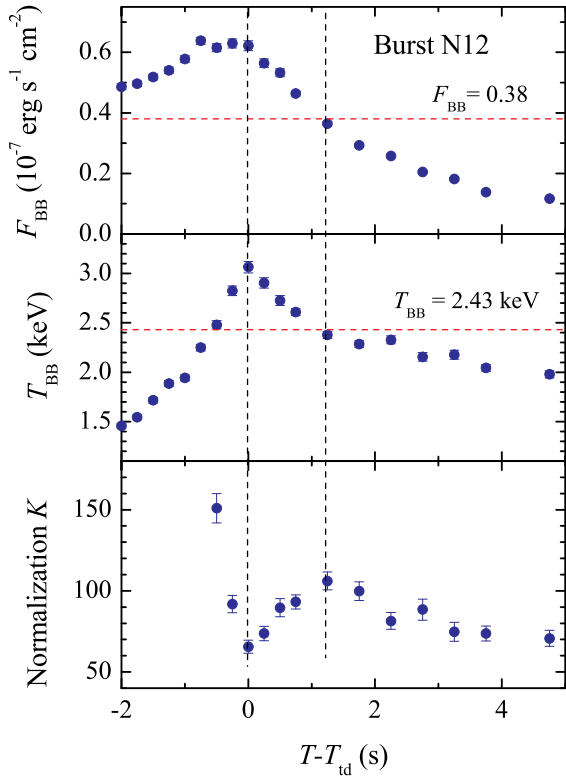
Figure 6. Results of the blackbody fits to the burst #12 (see also Fig. 5 and Table 2). The blackbody flux F_{BB}, temperature T_{BB} and normalization K in units of $(km/10\,kpc)^2$ are shown. The points between the vertical dashed lines were used for the direct cooling method.

are close to the knee point in the F_{BB}–kT_{BB} dependence, which was found by García et al. (2013).

The properties of the persistent state prior to the onset of all 16 short observed bursts from 4U 1820−30 are presented in Table 2. Kajava et al. (2014) demonstrated that X-ray bursts suitable for constraining NS parameters have significant evolution of the normalization after the photospheric touchdown point. It approxi-

mately doubles from the touchdown to the moment when the flux is half the touchdown flux F_{td}. In the considered bursts, the normalization reaches maximum values K_{max} at the flux of about 0.7 F_{td}, and we used the ratio K_{max}/K_{td} as a parameter describing the evolution of the normalization. This value is also shown for every burst in Table 2.

The burst fluences also contain potentially important information. Cumming (2003) showed that pure helium burning gives burst fluences independent on the persistent flux, whereas a relatively small amount of hydrogen ($X = 0.1$) together with heavy element abundances $Z = 0.01$ in the burning matter makes bursts more energetic at low persistent fluxes. The observed dependence is shown in Fig. 7 (top panel), and it is rather flat supporting pure helium burning in this source. The burst # 16 with a very unusually low fluence took place in a soft end of the hard persistent state and a rather high persistent flux (see Table 2 and Fig. 1). Possibly, part of the helium was burnt in the persistent regime before this burst.

Cumming (2003) also predicted another dependence, between the fluence and the recurrence time between bursts. Unfortunately, the *RXTE* observational sample consists of only two pairs of successive bursts. Therefore, we can find the recurrence time for two bursts only, namely bursts # 11 and 14. They are 4.16 and 1.89 h, corresponding to the persistent fluxes of 3.5×10^{-9} and 5.8×10^{-9} erg s^{-1} cm^{-2}. The shortening of the recurrence time is consistent with the results presented by Clark et al. (1977) and Haberl et al. (1987). Formally, the result is in accordance to the hydrogen–helium mix with solar chemical abundances of heavy elements (see the bottom panel of Fig. 7). However, it is obvious that it is just the result of small numbers of the observed points (compare with the top panel of the same figure). The corresponding α values for these two bursts, 125 ± 10 and 110 ± 10, are in a good agreement with results presented by Haberl et al. (1987).

3 APPLICATION OF THE DIRECT COOLING TAIL METHOD

The direct cooling tail method is based on an extended grid of the hot NS model atmospheres computed for a wide range of surface gravities (log g from 13.7 till 14.9 with the step 0.15), relative

Table 2. Parameters of the persistent emission before the bursts and burst fluences.

N	Obs. id.	Date MJD	K_{max}/K_{td}	HC	SC	Γ	kT (keV)	F_{per} (10^{-9} erg s^{-1}cm^{-2})	Fluence (10^{-7} erg cm^{-2})
1*	20075-01-05-00	50570.731795	1.53 ± 0.15	0.66	1.15	2.33 ± 0.04	2.33 ± 0.04	3.58 ± 0.04	3.25 ± 0.17
2*	40017-01-24-00	52794.738826	1.63 ± 0.13	0.92	1.22	1.93 ± 0.03	2.18 ± 0.08	2.80 ± 0.02	3.63 ± 0.25
3*	70030-03-04-01	52802.076265	1.55 ± 0.14	0.93	1.24	1.83 ± 0.03	2.01 ± 0.06	2.86 ± 0.02	3.87 ± 0.19
4*	70030-03-05-01	52805.896358	1.73 ± 0.14	0.84	1.25	2.06 ± 0.03	2.41 ± 0.06	3.74 ± 0.02	3.87 ± 0.23
5*	90027-01-03-05	53277.439257	1.42 ± 0.12	0.61	1.13	2.45 ± 0.05	2.31 ± 0.03	3.64 ± 0.02	3.61 ± 0.21
6	94090-01-01-02	54948.821939	1.50 ± 0.25	0.80	1.21	2.00 ± 0.06	2.18 ± 0.10	3.34 ± 0.04	3.72 ± 0.38
7*	94090-01-01-05	54950.703513	1.38 ± 0.14	0.94	1.26	1.86 ± 0.03	2.19 ± 0.10	3.44 ± 0.05	3.64 ± 0.26
8*	94090-01-02-02	54958.740672	1.73 ± 0.18	1.07	1.27	1.69 ± 0.05	1.93 ± 0.16	3.01 ± 0.04	3.64 ± 0.34
9	94090-01-02-03	54956.775426	1.90 ± 0.32	1.12	1.29	1.77 ± 0.04	2.14 ± 0.14	3.14 ± 0.04	3.77 ± 0.34
10	94090-01-04-00	54978.322182	1.83 ± 0.34	1.14	1.28	1.70 ± 0.05	2.00 ± 0.17	3.50 ± 0.04	4.07 ± 0.39
11	94090-01-04-01	54978.495588	1.48 ± 0.29	1.29	1.21	1.68 ± 0.04	2.00 ± 0.20	3.53 ± 0.04	4.19 ± 0.36
12*	94090-01-05-00	54981.187938	1.62 ± 0.13	1.13	1.35	1.71 ± 0.03	2.33 ± 0.09	3.83 ± 0.03	3.82 ± 0.57
13	94090-02-01-00	54994.534879	1.38 ± 0.25	0.87	1.29	2.04 ± 0.04	2.53 ± 0.09	5.64 ± 0.05	3.71 ± 0.56
14	94090-02-01-00	54994.613713	1.18 ± 0.13	0.82	1.24	2.12 ± 0.03	2.51 ± 0.05	5.80 ± 0.03	3.60 ± 0.44
15	96090-01-01-00	55624.881378	1.84 ± 0.23	0.91	1.22	1.95 ± 0.06	2.34 ± 0.17	2.89 ± 0.04	4.04 ± 0.59
16	96090-01-01-02	55626.774306	1.27 ± 0.14	0.51	1.01	2.55 ± 0.04	2.08 ± 0.03	4.69 ± 0.03	2.56 ± 0.12

Note: The persistent emission prior to the burst is characterized by the power-law index Γ and blackbody temperature kT, the hard (HC) and the soft (SC) colours and the flux. The bursts themselves are characterized by the ratio of the maximum blackbody normalization to that at the touchdown. The eight bursts, which are taken for analysis, are marked by a star. Errors are 1σ.
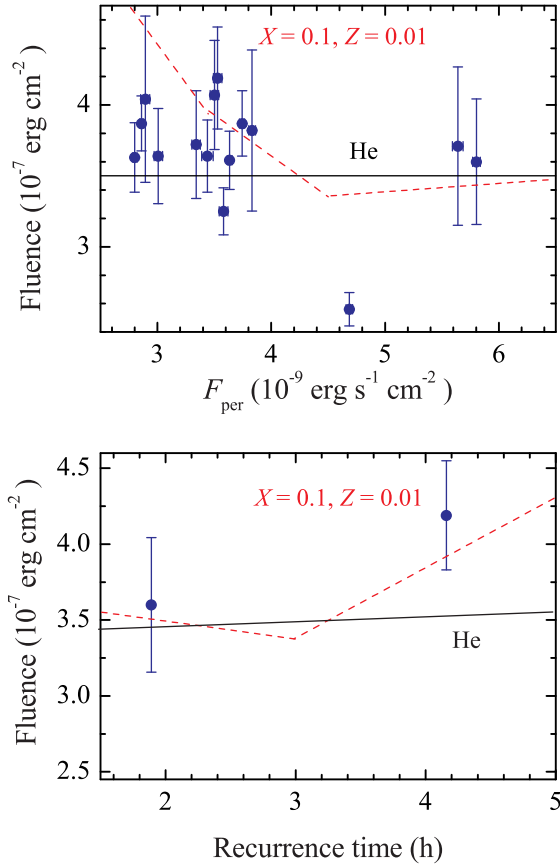
Figure 7. Dependences of the burst fluence on the persistent flux before the burst (top panel) and the recurrence time between bursts (bottom panel). The model curves for pure helium burning (solid curve) as well as burning of helium with some mixture of hydrogen and heavy elements (dashed red curves) were computed by Cumming (2003).

luminosities (from the actual Eddington limit to 0.1 $L_{\rm Edd}$) and various atmosphere chemical compositions (Suleimanov et al. 2012, 2017). The emergent model spectra $\mathcal{F}_{\rm E}$ were fitted with a diluted blackbody $B_{\rm E}$ in the observed energy band $3-20$ keV as

$$\mathcal{F}_{\rm E} \approx w\,\pi B_{\rm E}(f_{\rm c}T_{\rm eff}), \tag{1}$$

where the model effective temperature $T_{\rm eff}$ is determined by the relative luminosity of the model $\ell = L/L_{\rm Edd}$, $T_{\rm eff} = \ell^{1/4}\,T_{\rm Edd}$. Here, $\sigma_{\rm SB}\,T_{\rm Edd}^4 = gc/\kappa_{\rm T}$ is a critical (Eddington) temperature on the NS surface, and $\kappa_{\rm T} \approx 0.2(1+X)\,{\rm cm}^2\,{\rm g}^{-1}$ is the electron scattering opacity. The pairs w, $f_{\rm c}$ were obtained for every computed model emergent spectrum. This kind of approximation was made because observed spectra of X-ray bursts are well fitted by blackbody spectra with temperature $T_{\rm BB}$ and normalization $K = R_{\rm BB}^2/d^2$ as parameters (see e.g. Galloway et al. 2008). Here, d is the distance to the source. These observed spectrum fit parameters can be easily compared with the model parameters w and $f_{\rm c}$ to obtain information about physical NS radius R.

It is possible to derive the required relation (Suleimanov et al. 2017)

$$K = w\left(\frac{R(1+z)}{d}\right)^2 = w\,\Omega, \tag{2}$$

and to show that the observed dependence K–$F_{\rm BB}$ has to be fitted with the model dependence w–$wf_{\rm c}^4\,\ell$ if the model of a passively cooling NS is acceptable for a given X-ray burst. The factor $wf_{\rm c}^4$

is an inverted bolometric correction arising due to fitting the model spectra with equation (1) (Suleimanov et al. 2017). There are two fitting parameters for this procedure: Ω, which is the angular dilution factor proportional to the solid angle occupied by the NS on the sky, and the observed Eddington flux $F_{\rm Edd,\infty} = L_{\rm Edd}/4\pi d^2(1+z)^2$, which are combined to the observed Eddington temperature

$$kT_{\rm Edd,\infty} = kT_{\rm Edd}/(1+z) = 9.81\,(F_{\rm Edd,-7}/\Omega)^{-1/4}\ {\rm keV}. \tag{3}$$

This temperature is independent of the source distance d and any errors in the absolute observed flux. Here, $F_{\rm Edd,-7}$ is the observed Eddington flux $F_{\rm Edd,\infty}$ in units of $10^{-7}\ {\rm erg\,s^{-1}\,cm^{-2}}$ and Ω in units of $({\rm km}/10\,{\rm kpc})^2$.

Formally, only the crossing point of the constant $T_{\rm Edd,\infty}$ curve with the constant $\log g$ curve, for which the model dependence w–$wf_{\rm c}^4\,\ell$ was computed, gives a correct solution. This is the reason why the direct cooling tail method was introduced to cover all the M–R plane. For every M and R pair, the gravitational redshift z, the surface gravity g and the Eddington luminosity $L_{\rm Edd}$ are known, if the chemical composition of the NS atmosphere is given. The model curve w–$wf_{\rm c}^4\,\ell$ for a specific surface gravity g could be interpolated among the nine computed $\log g$ dependences and used for fitting the observed K–$F_{\rm BB}$ curve. In the considered case, the fitting parameters Ω and $F_{\rm Edd,-7}$ depend on the source distance d only, which is, therefore, the only fitting parameter of the method. The value of χ^2 is used as a measure of the fitting accuracy. Using this approach, we can get a χ^2 map in the M–R plane and find the regions with the minimum of χ^2 and the confidence regions containing the correct (M, R) pair with the likelihood, say, of 68, 95 and 99 per cent.

Selecting the part of the observed K–$F_{\rm BB}$ dependence, which is used for the fitting, could be crucially important for the method. The physically motivated truncation of the whole observed dependence at high fluxes is the touchdown point. It is commonly accepted that the photospheric radius equals to the NS radius at later burst cooling phases. Therefore, we use the points with bolometric fluxes $F_{\rm BB}$ less than the touchdown point flux. Determination of the cut-off boundary at low fluxes is much less obvious. We expect that accretion can restart sometime after the PRE phase and disturb the NS atmosphere, breaking the assumption of a passively cooling NS. The accretion rate during the burst actually can be even higher than before it (Worpel et al. 2013, 2015; Ji et al. 2014). In our previous work (Nättilä et al. 2016), we tried to find the bursts, which took place at very low persistent luminosities to minimize the influence of accretion. This approach is valid if we want to find the most accurate limits on NS masses and radii. Here, however, our aim is different. We wish to demonstrate that the cooling tail method gives the correct chemical composition of the NS atmosphere. Because of the rather high persistent flux of the source (about $0.07\,L_{\rm Edd}$) in the hard state, we have to limit our data to a short part of the cooling phase at high flux levels where theoretical atmosphere models describe the data. At lower fluxes, deviations become obvious because of a likely significant influence of the restarting accretion on to the observed burst properties (see Fig. 8).

We chose eight bursts for analysis, marked by stars in Table 2. They were chosen among others because they have the largest ratio $K_{\rm max}/K_{\rm td}$ with sufficient quality of the fitting, making them likely to follow theoretical atmosphere models (Kajava et al. 2014; Poutanen et al. 2014). Their observed dependences K–$F_{\rm BB}$ are shown in Fig. 8 together with the model curves w–$wf_{\rm c}^4\,\ell$ computed for $\log g = 14.3$ and two chemical compositions, pure helium and solar H/He mix. The found best-fitting parameters Ω and $F_{\rm Edd,-7}$ are also given. The observed points at the fluxes below $4 \times 10^{-8}\ {\rm erg\,s^{-1}\,cm^{-2}}$ deviate from the model curve significantly, and we excluded them
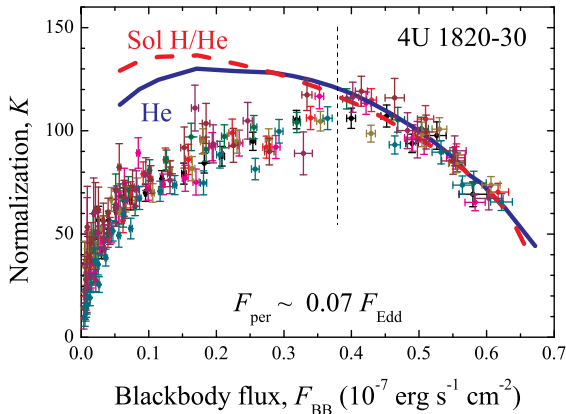
Figure 8. The observed K–F_{BB} dependence (circles with error bars) for the cooling tail (after touchdown) of the selected bursts of 4U 1820−30. The blue solid curve is the best-fitting theoretical dependence $w - w f_c^4 \ell$ for pure helium and $\log g = 14.3$ corresponding to the selected data (points to the right-hand side of the vertical dashed line with $F_{BB} > 0.38 \times 10^{-7}\,\mathrm{erg\,s^{-1}\,cm^{-2}}$). The fit parameters of the curve are $\Omega = 500\,(\mathrm{km}/10\,\mathrm{kpc})^2$ and $F_{Edd} = 0.596 \times 10^{-7}\,\mathrm{erg\,s^{-1}\,cm^{-2}}$. The red dashed curve is the best-fitting theoretical dependence for the solar hydrogen to helium abundance ratio and $\log g = 14.3$, with parameters $\Omega = 618\,(\mathrm{km}/10\,\mathrm{kpc})^2$ and $F_{Edd} = 0.596 \times 10^{-7}\,\mathrm{erg\,s^{-1}\,cm^{-2}}$.

from the analysis. The used points occupy a very short (about 1 s) time interval during the bursts and this interval is shown in Fig. 6. We cannot expect very high accuracy from these data, but it could be enough to demonstrate that the pure helium models give an acceptable result. We note that usage of all bursts give almost the same confidence regions at the M–R plane, but with a more irregular structure.

The results obtained by the direct cooling method are shown in Fig. 9. The confidence regions are situated along the whole $T_{Edd, \infty}$ curve, found for the fixed $\log g = 14.3$, with the χ^2 minimum at $R \approx 11$ km and $M \approx 1.45\,\mathrm{M_\odot}$ for pure He composition. The curves of constant distances of 6.5, 7 and 7.5 kpc are also shown. The most probable distance to the source is about 6.5 kpc. This value is smaller than the commonly accepted distance to NGC 6624 of 7.6 ± 0.4 kpc (Kuulkers et al. 2003), although earlier investigations (Vacca, Lewin & van Paradijs 1986) gave smaller distances, down to 6 kpc.

The NS radius obtained here for a $1.5\,\mathrm{M_\odot}$ NS is smaller than the radii obtained in our previous work (Nättilä et al. 2016) for other sources. We suggest two reasons for this difference. First, if the most distant acceptable solutions have a higher probability, our preferable solution will shift to larger radii 11–12 km and masses 1.8–2 $\mathrm{M_\odot}$. Such radii are in a good agreement with those derived by Nättilä et al. (2016). The NS mass could be high enough because of the long accretion history. Secondly, the analysed bursts happened at a rather large persistent luminosity of about $0.07 L_{Edd}$ (Kajava et al. 2014), whereas Nättilä et al. (2016) considered bursts at lower persistent luminosities $<0.02 L_{Edd}$. Accretion during the bursts disturbs the NS atmosphere affecting the observed K–F_{BB} dependence not only at low fluxes but even close to the touch-down. Our preliminary study (Suleimanov et al., in preparation) indicates that additional heating of the atmosphere top layers increases the colour-correction factor f_c, resulting in a shift of the M–R solution to larger radii by about 1 km. If the NS mass is as low as $1.35\,\mathrm{M_\odot}$ (Zdziarski et al. 2007), then the corresponding NS radius would be 11 ± 0.5 km.

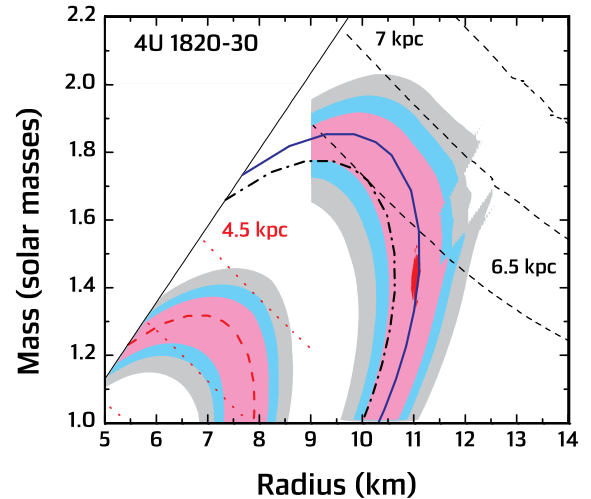Many authors tried to limit mass and radius of the NS in 4U 1820−30. van Paradijs & Lewin (1987) obtained an allowed

Figure 9. The χ^2 confidence regions (68, 90 and 99 per cent probabilities) in the mass–radius plane for 4U 1820−30 obtained using the direct cooling tail method for pure helium (right-hand regions with larger radii) and for the solar H/He abundance ratio (left-hand regions) model atmospheres. The best-fitting region for the He solution is marked by red. The minimum value of χ^2 is 34.6 for 31 dof. The corresponding values for the best-fitting solution using the solar H/He ratio are 36.9/31. The blue solid curve corresponds to the best-fitting $T_{Edd, \infty}$ (equation 3) for pure helium, the red dashed curve for the solar H/He atmospheres and the black dot–dashed curve for the atmospheres computed for $X = 0.1$, $Y = 0.9$ mix. All the curves were obtained for $\log g = 14.3$. The black dashed curves correspond to the constant distances of 6.5, 7.0 and 7.5 kpc (solutions for pure helium), and the red dotted curves correspond to the constant distances of 3.5, 4.0 and 4.5 kpc (solution for solar H/He mix). Solutions in the upper left-hand corner are forbidden because of general relativity effects.

region in the M–R plane close to ours when assuming a helium NS atmosphere and an anisotropy factor of $\xi = 1$. Shaposhnikov & Titarchuk (2004) investigated the decay phase of 4U 1820−30 bursts using their analytical representation of the f_c and obtained results, which are close to ours: $M \approx 1.3$–$2.0\,\mathrm{M_\odot}$ and $R \approx 11$–13 km, assuming the distance to the source between 5.8 and 7.0 kpc. The limitations derived by Kuśmierek, Madej & Kuulkers (2011) are very wide ($M = 1.3 \pm 0.6\,\mathrm{M_\odot}$, $R = 11^{+3}_{-2}$ km), but they include our confidence regions, too. Güver et al. (2010) reported a very high accuracy of the NS mass and radius, assuming a pure He composition ($M = 1.58 \pm 0.06\,\mathrm{M_\odot}$, $R = 9.1 \pm 0.4$ km). However, their method was not self-consistent, as shown by Steiner, Lattimer & Brown (2010) and Suleimanov et al. (2011b). In particular, the variations of the normalization K were ignored and only an averaged value was used. On the other hand, they took f_c values from the model atmosphere computations ignoring the fact that f_c and, therefore, K as well have to vary with the decreasing burst flux. Steiner et al. (2010) also remarked that the solutions obtained by Güver et al. (2010) were possible only with a probability of about 10^{-7}–10^{-8}. The recent re-analysis by Özel et al. (2016) included additional correction factors and significantly higher uncertainties of the K and $F_{Edd, \infty}$ measurements together with much wider possible errors for the distance. However, their new results are still plagued by the aforementioned inconsistencies because they kept the same approach as in Güver et al. (2010). As a result of the (artificially) expanded measurement errors, they obtained much wider limits for the NS mass and radius (1.3–2.2 $\mathrm{M_\odot}$ and 8–14 km), which include our confidence regions as well.

Assuming a solar H/He mix for the NS atmosphere composition, we obtain NS radii below 9 km (see lower left-hand side contours in

Fig. 9). Such radii are physically unrealistic (e.g. fig. 3 in Lattimer & Prakash 2016). This solution also corresponds to a too small distance to the source of about 4 kpc. Therefore, the data here are very strongly disfavouring the solar composition. This result is not affected by the uncertainties in the colour correction caused by ongoing accretion, as it is more robust under small changes in the observables. This is because $F_{\rm Edd} \propto 1/(1 + X)$ and, as such, is a strong function of the hydrogen mass fraction.

Actually all the solutions between the solar H/He mix solution and the pure He solution shown in Fig. 9 are possible, if we consider the H/He ratio as a free parameter. For instance, we computed a set of model atmospheres with $X = 0.1$ and $Y = 0.9$ for a fixed $\log g = 14.3$ because $X = 0.1$ is an upper limit for the hydrogen mass fraction in 4U 1820−30 (Cumming 2003). The model curve $w-wf_c^4 \ell$ fits well the observed K–$F_{\rm BB}$ curve with the parameters $\Omega = 530 \, ({\rm km}/10 \, {\rm kpc})^2$ and $F_{\rm Edd} = 0.6 \times 10^{-7} \, {\rm erg \, s^{-1} \, cm^{-2}}$. The curve corresponding to the obtained $T_{\rm eff,\infty}$ is shown in Fig. 9. We conclude that the existing uncertainty of the chemical composition of the accreting matter in 4U 1820−30 can shift the obtained limitations on the NS radius to lower values by the value of the statistical error.

We would like to emphasize that the accurate NS mass and radius determination was not the main goal of this work: 4U 1820−30 is not an ideal source for this purpose because of the high persistent flux level during the bursts. The main aim of the work was the demonstration of the potential power of the direct cooling method, which can give acceptable results even for such a complex X-ray bursting NS. The method also confirmed that the accreting matter in 4U 1820−30 is likely composed of pure He only.

4 SUMMARY

We presented our re-analysis of *RXTE* observations of the ultracompact X-ray bursting LMXB 4U 1820−30 and confirmed that almost all detected X-ray bursts took place during hard persistent states. Therefore, the cooling tail method can be used for analysis of these X-ray bursts to constrain the NS basic parameters. This source is not ideal for the method because of a relatively high persistent accretion rate ($\sim$0.04–0.09 $L_{\rm Edd}$) and a possible effect of the re-starting accretion on the spectral burst evolutions at the late cooling phases. We undertook this attempt mainly for demonstrating the method advantages and confirming that it gives the correct chemical composition of the accreting matter. The source is one of the best established binaries with a helium secondary, and we demonstrated that for pure helium composition the cooling tail method constrains the NS radius to be 11 ± 1 km for a low-mass ($M < 1.7 \, M_{\odot}$) star and radii in the range 8–12 km are possible for higher assumed masses. We also find that the obtained solutions for the solar H/He mix result in a too small ($< 9 \, {\rm km}$) NS radius and therefore can be excluded with a high degree of certainty. We have demonstrated using the cooling tail method that only a helium-dominated chemical composition of the NS atmosphere in 4U 1820−30 gives an NS mass and radius close to the canonical values for NSs. The uncertainties of the obtained M and R are, however, too large to produce serious limitations on the EoS in NS cores. The likely reason for that is the rather high persistent mass accretion rate, which can disturb the NS atmosphere and affect our results.

ACKNOWLEDGEMENTS

We acknowledge the anonymous referee, whose comments allowed us to improve the paper. The work was supported by the German

REFERENCES

Arnaud K. A., 1996, in Jacoby G. H., Barnes J., eds, ASP Conf. Ser. Vol. 101, ADASS V. Astron. Soc. Pac., San Francisco, p. 17
Bildsten L., 1998, in Buccheri R., van Paradijs J., Alpar A., eds, NATO Advanced Science Institutes (ASI) Series C Vol. 515, The Many Faces of Neutron Stars. Kluwer Academic Publishers, Dordrecht, p. 419
Chou Y., Grindlay J. E., 2001, ApJ, 563, 934
Clark G. W., Li F. K., Canizares C., Hayakawa S., Jernigan G., Lewin W. H. G., 1977, MNRAS, 179, 651
Costantini E. et al., 2012, A&A, 539, A32
Cumming A., 2003, ApJ, 595, 1077
Cumming A., 2004, Nucl. Phys. B, 132, 435
Damen E., Magnier E., Lewin W. H. G., Tan J., Penninx W., van Paradijs J., 1990, A&A, 237, 103
Ebisuzaki T., 1987, PASJ, 39, 287
Galloway D. K., Muno M. P., Hartman J. M., Psaltis D., Chakrabarty D., 2008, ApJS, 179, 360
García F., Zhang G., Méndez M., 2013, MNRAS, 429, 3266
Gilfanov M., Revnivtsev M., Molkov S., 2003, A&A, 410, 217
Grindlay J., Gursky H., Schnopper H., Parsignault D. R., Heise J., Brinkman A. C., Schrijver J., 1976, ApJ, 205, L127
Güver T., Wroblewski P., Camarota L., Özel F., 2010, ApJ, 719, 1807
Haberl F., Stella L., White N. E., Gottwald M., Priedhorsky W. C., 1987, ApJ, 314, 266
Haensel P., Potekhin A. Y., Yakovlev D. G., 2007, Astrophysics and Space Science Library Vol. 326, Neutron Stars 1: Equation of State and Structure. Springer, New York
Heasley J. N., Janes K. A., Zinn R., Demarque P., Da Costa G. S., Christian C. A., 2000, AJ, 120, 879
Iben I. Jr., Tutukov A. V., 1991, ApJ, 370, 615
in't Zand J. J. M., Weinberg N. N., 2010, A&A, 520, A81
in't Zand J. J. M., Homan J., Keek L., Palmer D. M., 2012, A&A, 547, A47
Inogamov N. A., Sunyaev R. A., 2010, Astron. Lett., 36, 848
Ji L. et al., 2013, MNRAS, 432, 2773
Ji L., Zhang S., Chen Y., Zhang S.-N., Torres D. F., Kretschmar P., Li J., 2014, ApJ, 791, L39
Kajava J. J. E. et al., 2014, MNRAS, 445, 4218
Kajava J. J. E., Nättilä J., Poutanen J., Cumming A., Suleimanov V., Kuulkers E., 2017, MNRAS, 464, L6
Kuśmierek K., Madej J., Kuulkers E., 2011, MNRAS, 415, 3344
Kuulkers E., den Hartog P. R., in't Zand J. J. M., Verbunt F. W. M., Harris W. E., Cocchi M., 2003, A&A, 399, 663
Lapidus I. I., Sunyaev R. A., Titarchuk L. G., 1986, Sov. Astron. Lett., 12, 383
Lattimer J. M., Prakash M., 2007, Phys. Rep., 442, 109
Lattimer J. M., Prakash M., 2016, Phys. Rep., 621, 127
Lattimer J. M., Steiner A. W., 2014, ApJ, 784, 123
Lewin W. H. G., van Paradijs J., Taam R. E., 1993, Space Sci. Rev., 62, 223
London R. A., Howard W. M., Taam R. E., 1984, ApJ, 287, L27
London R. A., Taam R. E., Howard W. M., 1986, ApJ, 306, 170
Madej J., 1991, ApJ, 376, 161
Nättilä J., Suleimanov V. F., Kajava J. J. E., Poutanen J., 2015, A&A, 581, A83
Nättilä J., Steiner A. W., Kajava J. J. E., Suleimanov V. F., Poutanen J., 2016, A&A, 591, A25

Özel F., 2006, Nature, 441, 1115

Özel F., Psaltis D., Güver T., Baym G., Heinke C., Guillot S., 2016, ApJ, 820, 28

Paczynski B., Anderson N., 1986, ApJ, 302, 1

Pavlov G. G., Shibanov I. A., Zavlin V. E., 1991, MNRAS, 253, 193

Poutanen J., Nättilä J., Kajava J. J. E., Latvala O.-M., Galloway D. K., Kuulkers E., Suleimanov V. F., 2014, MNRAS, 442, 3777

Postnov K. A., Shakura N. I., 1987, Sov. Astr. Lett., 13, 122

Priedhorsky W., Terrell J., 1984, ApJ, 284, L17

Rappaport S., Ma C. P., Joss P. C., Nelson L. A., 1987, ApJ, 322, 842

Rauch T., Suleimanov V., Werner K., 2008, A&A, 490, 1127

Revnivtsev M. G., Suleimanov V. F., Poutanen J., 2013, MNRAS, 434, 2355

Shaposhnikov N., Titarchuk L., 2004, ApJ, 606, L57

Steiner A. W., Lattimer J. M., Brown E. F., 2010, ApJ, 722, 33

Stella L., Priedhorsky W., White N. E., 1987, ApJ, 312, L17

Strohmayer T., Bildsten L., 2006, in Lewin W., van der Klis M., eds, Compact stellar X-ray sources, Cambridge Astrophysics Series, No. 39. Cambridge Univ. Press, Cambridge, p. 113

Strohmayer T. E., Brown E. F., 2002, ApJ, 566, 1045

Suleimanov V., Poutanen J., Werner K., 2011a, A&A, 527, A139

Suleimanov V., Poutanen J., Revnivtsev M., Werner K., 2011b, ApJ, 742, 122

Suleimanov V., Poutanen J., Werner K., 2012, A&A, 545, A120

Suleimanov V. F., Poutanen J., Klochkov D., Werner K., 2016, Eur. Phys. J. A, 52, 20

Suleimanov V. F., Poutanen J., Nättilä J., Kajava J. J. E., Revnivtsev M. G., Werner K., 2017, MNRAS, 466, 906

Vacca W. D., Lewin W. H. G., van Paradijs J., 1986, MNRAS, 220, 339

van Paradijs J., Lewin W. H. G., 1987, A&A, 172, L20

van Paradijs J., Dotani T., Tanaka Y., Tsuru T., 1990, PASJ, 42, 633

Weinberg N. N., Bildsten L., Schatz H., 2006, ApJ, 639, 1018

Worpel H., Galloway D. K., Price D. J., 2013, ApJ, 772, 94

Worpel H., Galloway D. K., Price D. J., 2015, ApJ, 801, 60

Zamfir M., Cumming A., Galloway D. K., 2012, ApJ, 749, 69

Zdziarski A. A., Wen L., Gierliński M., 2007, MNRAS, 377, 1006

This paper has been typeset from a TEX/LATEX file prepared by the author.